Direct evidence of real-space pairing in $BaBiO_3$

A. P. Menushenkov,[1,*] A. Ivanov,[1] V. Neverov,[1] A. Lukyanov,[1] A. Krasavin,[1] A. A. Yastrebtsev,[1] I. A. Kovalev,[1] Y. Zhumagulov,[2] A. V. Kuznetsov,[1] V. Popov,[1] G. Tselikov,[3] I. Shchetinin,[4] O. Krymskaya,[1] A. Yaroslavtsev,[5] R. Carley,[6] L. Mercadier,[6] Z. Yin,[6] S. Parchenko,[6] L. P. Hoang,[6] N. Ghodrati,[6] Y. Y. Kim,[6] J. Schlappa,[6] M. Izquierdo,[6] S. Molodtsov,[6,7,8] and A. Scherz[6]

[1]*National Research Nuclear University MEPhI (Moscow Engineering Physics Institute), Moscow 115409, Russia*

[2]*University of Regensburg, Regensburg 93040, Germany*

[3]*Emerging Technologies Research Center, XPANCEO, Internet City, Emmay Tower, Dubai 00000, United Arab Emirates*

[4]*National University of Science and Technology MISiS, Moscow 119049, Russia*

[5]*Department of Physics and Astronomy, Uppsala University, Uppsala 75120, Sweden*

[6]*European XFEL GmbH, Schenefeld 22869, Germany*

[7]*Institute of Experimental Physics, TU Bergakademie Freiberg, Leipziger Strasse 23, 09599 Freiberg, Germany*

[8]*Center for Efficient High Temperature Processes and Materials Conversion (ZeHS), TU Bergakademie Freiberg, Winklerstrasse 5, 09599 Freiberg, Germany*

(Received 13 December 2023; revised 29 March 2024; accepted 17 May 2024; published 21 June 2024)

The parent compound $BaBiO_3$ of bismuthate high-temperature superconductors (HTSCs) $BaBi(Pb)O_3$ and $Ba(K)BiO_3$ with perovskitelike structure exhibits unusual electronic and structural properties, which can be satisfactorily explained if we assume that all charge carriers are in the paired state. However, the prior experiments and the first-principle calculations only indirectly indicate the existence of paired charge carriers in $BaBiO_3$. In this work, we report the direct evidence of initially paired electrons and holes in the upper antibonding Bi $6s$−O $2p_{\sigma^*}$ orbital of the neighboring octahedral complexes in the ground state of $BaBiO_3$ using the time-resolved x-ray absorption spectroscopy (XAS) to monitor the electron dynamics after the femtosecond resonant 633 nm laser excitation. We observe strong changes in the oxygen K-edge XAS preedge region, defined by the Bi $6s$−O $2p_{\sigma^*}$ orbitals. We interpret them as a fast ($\leqslant$0.3 ps) breaking of charge carrier pairs and slower (0.3–0.8 ps) lattice rearrangement from the distorted monoclinic structure into the new metastable state with a cubic lattice, which persists at least up to 60 ps after the excitation. Analysis of the intermediate state at the fast excitation shows that the bond disproportionation and monoclinic distortion of $BaBiO_3$ structure are energetically favorable due to the charge carrier pairing. Thus the compound $BaBiO_3$ forms a new quantum state that we define as a local pair density wave. Taking into account a large number of similarities between bismuthate and cuprate high-temperature superconductors, we believe that our work will give a new impetus to understanding the nature of superconductivity in perovskite HTSCs.

DOI: 10.1103/PhysRevResearch.6.023307

I. INTRODUCTION

In recent years, $BaBiO_3$, the parent compound of the bismuthate high-temperature superconductor (HTSC) family ($Ba_{1-x}K_xBiO_3$ and $BaPb_{1-x}Bi_xO_3$) has attracted a new wave of interest from both theoretical and experimental condensed matter communities (see the review [1] and references therein). This is partially due to the observation of a topological state in $BaBiO_3$ [1–4] predicted by Yan *et al.* [5]. But the main interest in this material is caused by the fact that a unified theory for the insulating state in the pure $BaBiO_3$ and superconductivity in the doped phases is still missing [1,2,6–13].

After the discovery of superconductivity in $BaPb_{0.25}Bi_{0.75}O_3$ at ∼13 K [14] and in $Ba_{0.6}K_{0.4}BiO_3$ at ∼30 K [15,16] the bismuthates have been studied extensively using state-of-the-art methods. However, a significant part of the unusual properties of the parent compound $BaBiO_3$, described already in the early review by Uchida *et al.* [17], have not consistently been explained so far.

Among the most important anomalies of this unique semiconductor, the review [17] emphasizes the following: the existence of two energy gaps—an optical gap $E_G \approx 1.96$ eV and transport (activation) gap $E_a \approx 0.24$ eV; the extraordinarily large value of the preexponential factor $n_0 = 1.1 \times 10^{22}$ cm^{-3}, equal to the number of unit cells per unit volume, obtained from the charge transport measurements for a concentration of itinerant charge carriers $n(T) = n_0 \exp(-E_a/kT)$; abnormally large amplitude of the breathing Raman mode (∼570 cm^{-1}) at the resonant laser excitation through the optical gap. Based on the summary of these

*Corresponding author: menushen@gmail.com

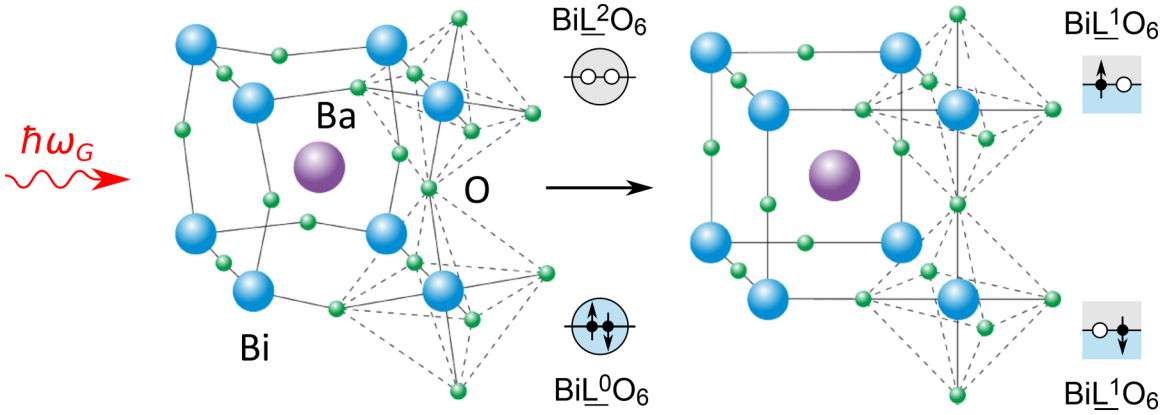

FIG. 1. Local crystal and electronic structure of $BaBiO_3$. Left: ground state with larger $Bi\underline{L}^0O_6$ and smaller $Bi\underline{L}^2O_6$ octahedra carrying the electron and hole pairs on the upper antibonding Bi $6s$–O $2p_{\sigma^*}$ orbital, respectively. Right: excited state after resonant laser excitation $\hbar\omega_G$ through the optical gap with broken pairs and equal octahedra. Circles denote paired states. $\underline{L}^2$, $\underline{L}^0$, and $\underline{L}^1$ denote a local hole pair, a local electron pair, and a single electron (hole), respectively.

observations it was suggested in [17] that unusual electronic and structural properties of $BaBiO_3$ can be satisfactorily explained if one assumes that all charge carriers are in the paired state and the conductivity is due to two-particle transport, possibly within the bipolaronic description. Thus the main question raised by the authors of [17] is the nature of the ground state in the parent compound. We believe that the answer to this question is the key to understanding not only the insulating state and the two-particle transport in $BaBiO_3$, but also the mechanism of superconductivity in the doped bismuthates.

The approaches explaining the insulating behavior of $BaBiO_3$ in the literature can be divided into two groups: charge disproportionation on the Bi sites and bond disproportionation per hybridization between the Bi $6s$ and O $2p$ orbitals. Both approaches lead to the appearance of breathing distortion in the $BaBiO_3$ perovskite lattice [1].

A few different models of Bi charge disproportionation $2Bi^{4+} \rightarrow Bi^{3+} + Bi^{5+}$ have been proposed [9,18–22]. However, this scenario does not agree with the results of photoemission spectroscopy, which showed no splitting of the Bi $4f$ core states [23–25]. Some of the electronic structure calculations using the linear-augmented-plane-wave (LAPW) [26,27] and density-functional-theory (DFT) [28,29] approaches also indicated the absence of a visible charge difference at two bismuth sites. To smooth over these contradictions, Rice's concept [20,30] of a local commensurate charge density wave (CDW) was proposed [17,26,27,31,32]. In addition, several models of charge disproportionation with noninteger bismuth valence $Bi^{4\pm\delta}$ ($0 < \delta < 1$) were considered [13,33].

Another approach, the so-called "bond disproportionation," based on the scheme $2Bi^{4+} \rightarrow Bi^{3+} + Bi^{3+}\underline{L}^2$, proposed for the first time in [34,35] (here $\underline{L}^2$ denotes two holes spread over the $2p$ orbitals of six oxygen atoms surrounding the Bi ion), does not contradict the photoemission spectroscopy results since both bismuth ions are in the same valence state Bi^{3+}. It was implemented in a variety of models [12,28,29,36–38] and is now regarded as the preferred one [1]. However, these models do not take into account the paired state of charge carriers [17] in the ground state of $BaBiO_3$ and consider the breathing lattice distortion [28] or different local environments of bismuth atoms [29] to be responsible for the bond disproportionation.

Besides, the above models do not explain the splitting of Bi $4f$ lines, observed in high-resolution photoelectron spectra [24] in the superconducting phase of $Ba_{1-x}K_xBiO_3$, which, from our point of view [39], indicates the appearance of two bismuth valence states upon doping in contrast to the initial $BaBiO_3$.

In our previous works based on EXAFS (extended x-ray absorption fine structure) [39,40] and XANES (x-ray absorption near edge structure) [34,35] experiments, we proposed the bond disproportionation model $2Bi\underline{L}^1O_6 \rightarrow Bi\underline{L}^0O_6 + Bi\underline{L}^2O_6$ that emphasizes the role of real-space pairing and may explain the anomalies of the $BaBiO_3$ ground state noted in [17]. In this model, the $Bi\underline{L}^2O_6$ is a small octahedron carrying the hole pair $\underline{L}^2$ and behaving as a rigid molecule with a vacant upper antibonding Bi $6s-$O $2p_{\sigma^*}$ orbital. $Bi\underline{L}^0O_6$ is a large soft octahedron carrying the electron pair and acting as an unstable molecule with a filled upper antibonding Bi $6s-$O $2p_{\sigma^*}$ orbital. It is the local pairing that produces the monoclinic distortion of a $BaBiO_3$ cubic lattice including breathing and tilting distortions. A local electron pair can tunnel between the neighboring complexes according to the dynamic exchange $Bi\underline{L}^2O_6 \leftrightarrow Bi\underline{L}^0O_6$, causing oxygen atom vibrations in a double-well potential. Resonant optical excitation through the optical gap $E_G \approx 1.96$ eV should lead to the local pair destruction and in the excited state $BaBiO_3$ represents a system of identical $Bi\underline{L}^1O_6$ octahedra with one electron and one hole in the upper Bi $6s-$O $2p_{\sigma^*}$ antibonding orbital [39] (Fig. 1).

Within such a point of view, the parent compound $BaBiO_3$ may also be considered as a system with real-space [41] or hardcore [42] bosons (i.e., with only one boson per site) using Anderson's concept of negative U' potential [20]. A number of works argue that the electron- and hole-pairing mechanism in $BaBiO_3$ has an electronic [42–44] rather than phononic (bipolaronic) [17,20,32,45,46] nature.

Our bond disproportionation model is in good agreement with the results of transport measurements, x-ray and neutron

diffraction, inelastic neutron and electron scattering, Raman scattering, and photoemission spectroscopy. By taking into account the conservation of the real space pairing occurring with the potassium doping of parent $BaBiO_3$ [39,47], it allowed us to propose a new scenario for the microscopic mechanism of superconductivity in $Ba_{1-x}K_xBiO_3$ (BKBO) based on the existence of spatially separated Fermi-Bose mixture [48,49].

However, our EXAFS and resonant Raman results [39,40,47] as well as other studies of optical conductivity, Raman scattering, and transport measurements discussed in [17] might be considered only an indirect proof of the local charge carrier pairing in the ground state of $BaBiO_3$.

In recent years x-ray free electron lasers (XFELs) have opened unique opportunities for time-resolved studies of charge order dynamics and the relationship between electronic, spin, and lattice degrees of freedom in the complex systems such as cuprate HTSCs [50–53]. The photoexcitations leading to the emergence of unique properties can be efficiently separated in space, time, and energy domains. In this work we use these capabilities in order to show direct evidence of initially paired carriers in $BaBiO_3$ forming a new quantum state of local pair-density wave (LPDW). We employ transient x-ray absorption spectroscopy (tr-XAS) to follow the electron dynamics driven by a femtosecond laser across the optical gap. The temporal evolution of different electronic and lattice states observed in tr-XAS clearly points to the existence of coupled local electron and hole pairs in the ground state of $BaBiO_3$.

II. RESULTS

We performed time-resolved oxygen *K*-edge x-ray absorption spectroscopy of photoexcited thin 90 nm $BaBiO_3$ films grown on 100 nm Si membrane substrates. The experiment was conducted at the Spectroscopy and Coherent Scattering (SCS) instrument of the European XFEL facility. All measurements were carried out at room temperature.

Figure 2(a) shows the experimental scheme for tr-XAS based on a beam-splitting off-axis zone plate (BOZ) creating three copies of the incoming beam [54], which are used to measure the transmitted intensity through the laser-excited and unexcited sample, as well as to monitor the incoming intensity with a pulse-resolved detector; see Appendix B. The sample was excited using 30 fs laser pulses centered at 1.96 eV (633 nm) and a pump fluence reaching 32 mJ/cm^2. The probe photon energy was scanned in the range of 525–550 eV [55] with a resolution of $\Delta E/E \sim 2 \times 10^{-4}$. The delay between the optical pump and the XFEL probe pulses was varied over a wide range from -1 ps to 60 ps. Thus we directly probed the changes and dynamics of the $BaBiO_3$ unoccupied density of states after the femtosecond laser pulse excitation through the optical gap $E_G \approx 1.96$ eV.

The oxygen *K*-edge XAS spectra of the ground and excited $BaBiO_3$ states are shown in Fig. 2(b). They consist primarily of the preedge peak around 529 eV, which is defined by the Bi $6s-$O $2p_{\sigma^*}$ antibonding orbital [red area in Fig. 2(b)], the shoulder at 531–533 eV, which corresponds to the O $2p-$Bi $6p$ hybridized states (green area), and the main peak at 533–535 eV, which is determined mainly by the O $2p$–Ba $5d$ hybridized states (blue area) [24,56].

In the bottom panel of Fig. 2(b) the differences between the spectra of excited state measured with the pump laser fluence 8 mJ/cm^2 and the spectra of ground state are shown for the different pump-probe delay times from -0.1 to 59.8 ps. First, one can see the positive and negative peaks appearing in the preedge region of the difference spectrum ΔXAS immediately after the excitation, which corresponds to the increase and the drop of XAS intensity at the rising edge and near the center of the preedge peak, respectively. These positive and negative contributions in ΔXAS, which we further denote as peaks A and B, are separated by $\sim$1 eV in energy and are visible already at 0 ps, showing the maximum amplitude at $\sim$0.2 ps, which is followed by a monotonous decay. Notably, within the first picosecond, from 0 to 0.8 ps after the excitation, the maximum of peak A shifts by $\sim$0.2 eV to the higher photon energy. This shift is shown in a greater detail in Figs. 2(c) and 2(d).

There are a few less pronounced negative and positive features in the difference spectrum in the energy region 531–533 eV. They become clearly visible at the delay time 0.1 ps and undergo intensity redistribution within the first picosecond after the excitation, with the negative feature disappearing shortly after 0.5 ps. At larger delay times the amplitudes of the remaining features change slightly.

In the energy range 533–535 eV of the difference spectrum no features are visible right after time zero. However, at the delay times 0.2–0.3 ps two weak minima appear in this range. Their amplitudes keep growing slowly and reach saturation between 0.8 and 1.8 ps.

Importantly, most of the above described spectral features do not disappear completely before the largest delay time of 59.8 ps reached in our experiment. This indicates that the system does not relax into the ground state at least up to 60 ps after the excitation and a new quasiequilibrium state forms.

We believe that the most important information about the rearrangement of the local electronic and crystal structures upon the excitation over the optical gap in $BaBiO_3$ is contained in the preedge region of XAS, since this energy range corresponds to the upper Bi $6s-$O $2p_{\sigma^*}$ antibonding orbital. The dependence of the preedge peak shape on the delay time after the resonant optical excitation appears in the difference spectrum as a change of the peak A and B amplitudes, positions, and widths [Fig. 2(b)]. It allows us to analyze the entire dynamics of the local electronic and crystal structure rearrangement in $BaBiO_3$. Therefore, the subsequent analysis will mainly focus on this spectral range.

The delay time evolution of the O *K*-edge XAS preedge peak at different optical pump fluences is shown in the top panel of Fig. 3. The maximum change of the preedge peak is observed at an early time (0.2 ps) after the excitation: the peak broadens and shifts to the lower photon energy side and its amplitude decreases strongly. At later times (0.8–4.8 ps) the peak restores its amplitude and shifts back to higher photon energy, but not completely, which points to the transition of the system to a new state. Notably, the peak shape at 4.8 ps is close to the shape at 0.8 ps, which means that the transition in the electronic and crystal structure is mostly complete already at the delay time of 0.8 ps. As excitation fluence increases, we

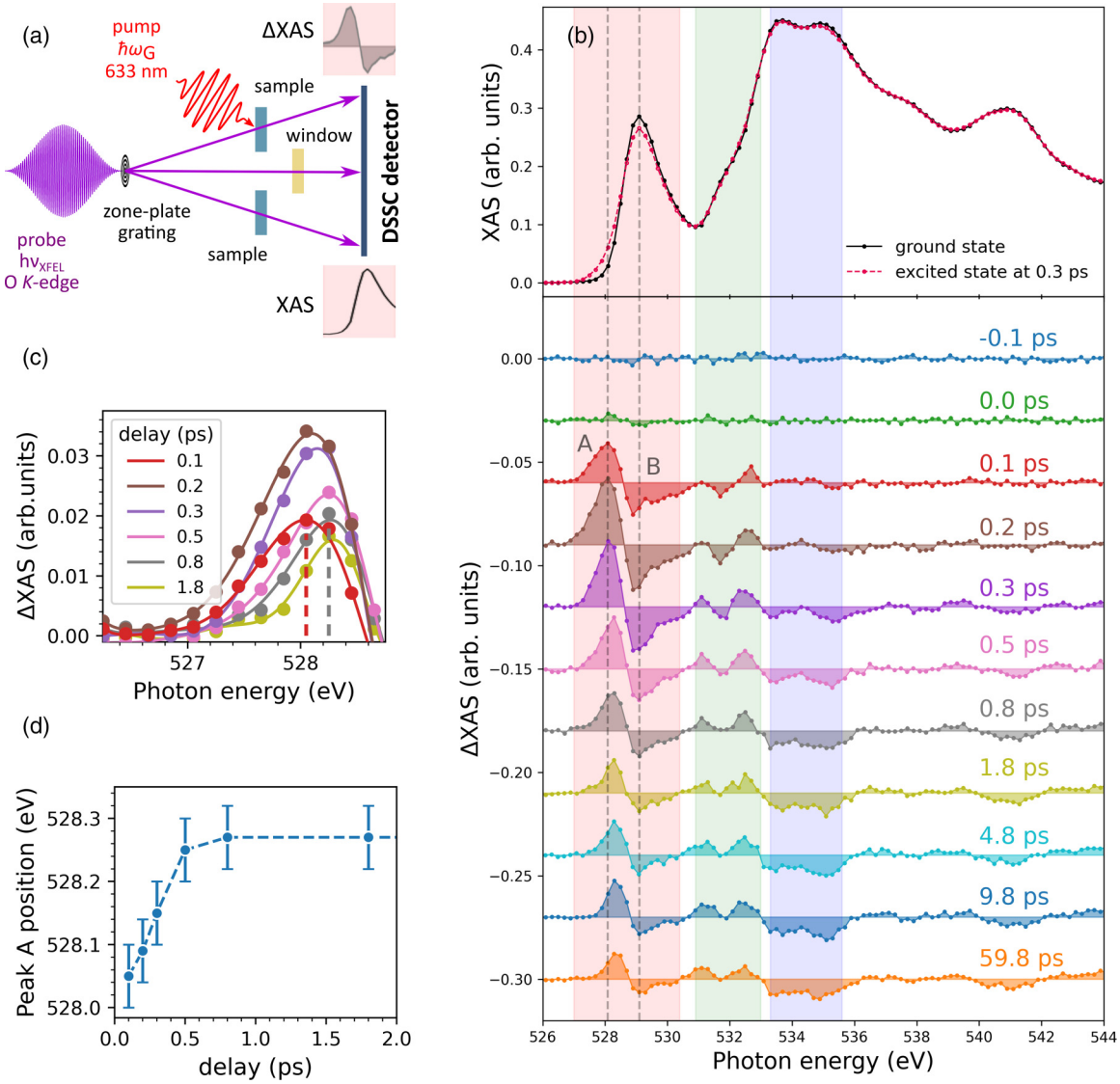

FIG. 2. Pump-induced excitation of $BaBiO_3$ ground state in the O *K*-edge XAS experiment at XFEL. (a) Schematics of the tr-XAS experiment at the SCS instrument. (b) Top panel: the experimental ground state (black line) and the excited state (red line) O *K* XAS of $BaBiO_3$ measured at the delay time 0.3 ps and optical pump fluence 8 mJ/cm^2. Three characteristic spectral ranges are marked with colors: (red) the pre-edge O *K* XAS peak corresponding to the Bi 6*s*–O $2p_{\sigma^*}$ antibonding orbital; (green) the rising edge of the main O *K* XAS peak corresponding to the hybridized O 2*p*−Bi 6*p* states; (blue) the main O *K* XAS peak corresponding to the hybridized O 2*p*−Ba 5*d* states (the "lattice" states). Bottom panel: the difference between the excited and ground state spectra ΔXAS of $BaBiO_3$ measured at the different delay times from −0.1 to 59.8 ps. The positive peak A and negative peak B in ΔXAS are marked with the vertical dashed lines. (c) The evolution of peak A in ΔXAS with the delay time changing from 0.1 to 1.8 ps. (d) The energy position of peak A *vs* the delay time.

see qualitatively similar effects in the preedge region, but they become stronger.

At times $\geqslant 0.8$ ps after the excitation the sample can be described as a mixture of excited and ground states of $BaBiO_3$, with the density of states (DOS) of each type giving a contribution to the XAS with a certain weight. The bottom panel of Fig. 3 shows the spectra measured at the delay time 4.8 ps fitted with the sum of DOS for the ground and excited states, calculated *ab initio* (see the Supplemental Material Fig. S1[57]). The ground state is characterized by a distortion of the ideal cubic perovskite lattice and two types of oxygen octahedrons. In the excited state, the octahedra transform into two identical ones and the lattice distortion disappears. Parameters of the ground state contribution in XAS (energy position and width) were found from the fit of the unexcited spectrum. The energy position of the excited state contribution in XAS was determined from the energy separation between the peak and the dip in the difference spectrum [Fig. 2(b)]. The weight of the excited state α was obtained from the spectra using the equation $\mathrm{XAS} = (1-\alpha)\mathrm{DOS}_{\mathrm{ground}} + \alpha\mathrm{DOS}_{\mathrm{excited}}$. It shows almost linear dependence vs the optical pump fluence (the inset in the bottom panel of Fig. 3). At the highest optical pump fluence 32 mJ/cm^2 applied in our experiment, the fraction of the excited state reaches 27%. In order to reduce the heat load and prevent damage of the thin film sample, most of the time-resolved measurements were performed at the pump fluence 8 mJ/cm^2, at which the fraction of the excited state is estimated as 5%.

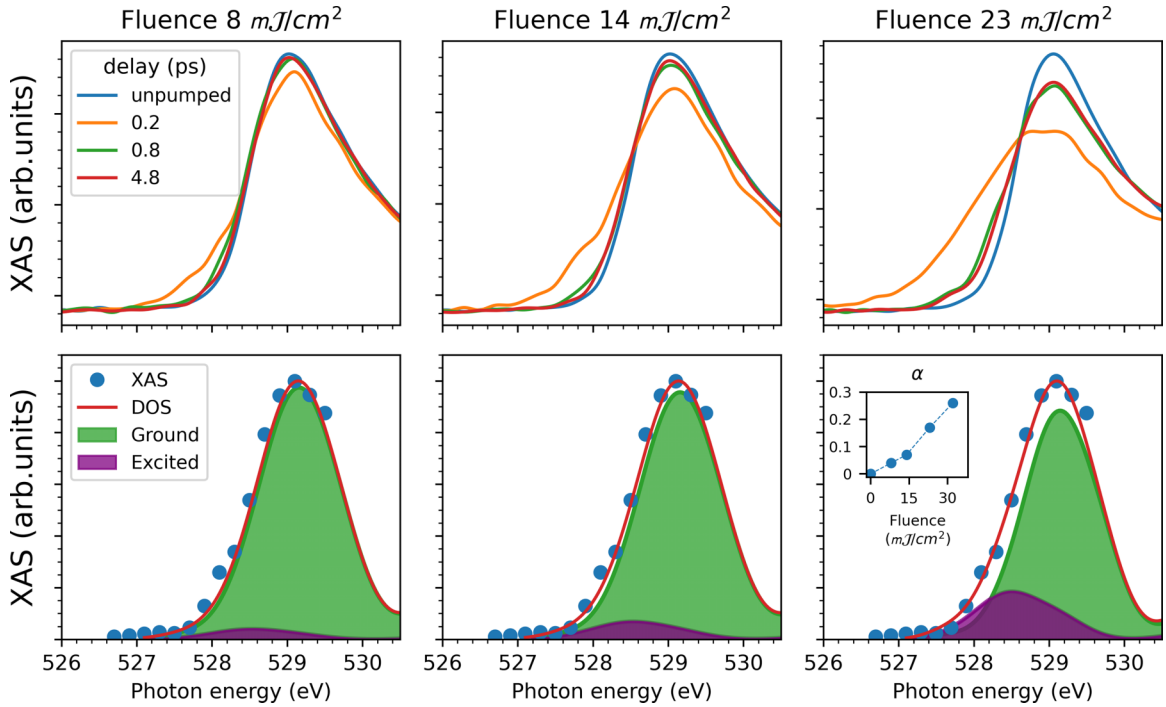

FIG. 3. Dynamics of $BaBiO_3$ *K* O XAS preedge peak. Top panel: the preedge peak of $BaBiO_3$ O *K* XAS measured at the ground (unpumped) state and different delay times after the excitation (0.2, 0.8, and 4.8 ps) at three optical pump fluences. Bottom panel: the experimental preedge XAS peak at the delay time 4.8 ps (blue circles) and its fitting (solid red line) with the sum of calculated ground (green) and excited (purple) state DOS. Inset in the bottom panel: the fraction of the excited state α in the resulting XAS spectrum *vs* the optical pump fluence.

In order to estimate the characteristic times of the local electronic and crystal structure rearrangement in $BaBiO_3$ after femtosecond resonant excitation over the optical gap we have used a three-exponential model [51]. Figure 4 shows a delay time scan measured at a fixed photon energy 528.2 eV, corresponding to the peak A in the difference spectrum ΔXAS, and its fitting with three exponents according to Eq. (1):

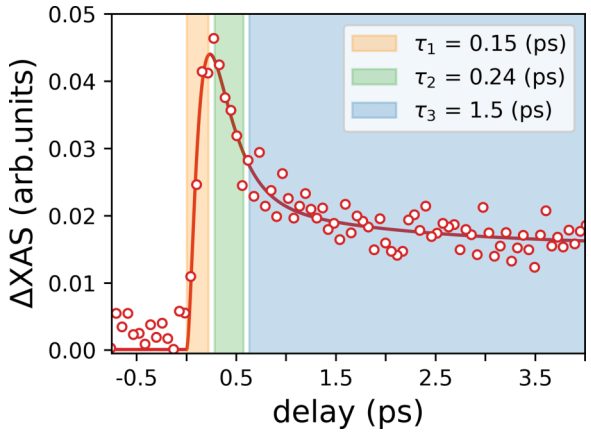

FIG. 4. Three-exponential fitting of time-dependent ΔXAS at the photon energy 528.2 eV (peak A). (Red circles) The delay time scan measured at the fixed photon energy 528.2 eV corresponding to the peak A in the difference spectrum ΔXAS and the pump fluence 8 mJ/cm^2. (Solid red line) Three-exponential fitting of the time scan. The time ranges where three characteristic processes give the biggest impact are marked with colors: (orange) electronic structure excitation, (green) electronic structure relaxation, and (blue) lattice rearrangement. Inset: three characteristic times obtained from the exponential fit.

$$\Delta\mathrm{XAS} = \left[\Theta(t-t_d)\left(1-e^{-\frac{t-t_d}{\tau_1}}\right)\right. \times \left.\left(A_1 + A_2 e^{-\frac{t-t_d}{\tau_2}} + A_3 e^{-\frac{t-t_d}{\tau_3}}\right)\right]^2. \quad (1)$$

From the fitting three characteristic times are obtained, which we relate to the fast excitation of the electronic subsystem right after the absorption of laser pulse $\tau_1 \sim 0.15$ ps, the relatively fast partial relaxation of the electronic subsystem back to the ground state $\tau_2 \sim 0.24$ ps, and the slower rearrangement of the lattice $\tau_3 \sim 1.5$ ps. Very similar characteristic times were also obtained from the analysis of the time delay scan measured at the photon energy 529.1 eV, corresponding to the negative peak B in ΔXAS (Fig. S2 in the Supplemental Material [57]). We note once again that the amplitude of both peaks A and B do not relax to zero at large delay times, which confirms the formation of a new state after excitation, stable at least on the tens of picoseconds time scale. More details about the three-exponential fitting procedure are given in Supplemental Material [57].

III. DISCUSSION

The temporal behavior of the difference spectrum ΔXAS [Figs. 2(b) and 2(c)] within the first picosecond after the resonant optical excitation may provide a direct confirmation that the charge carriers in the ground state of $BaBiO_3$ exist in the form of electron and hole pairs, localized in the large and

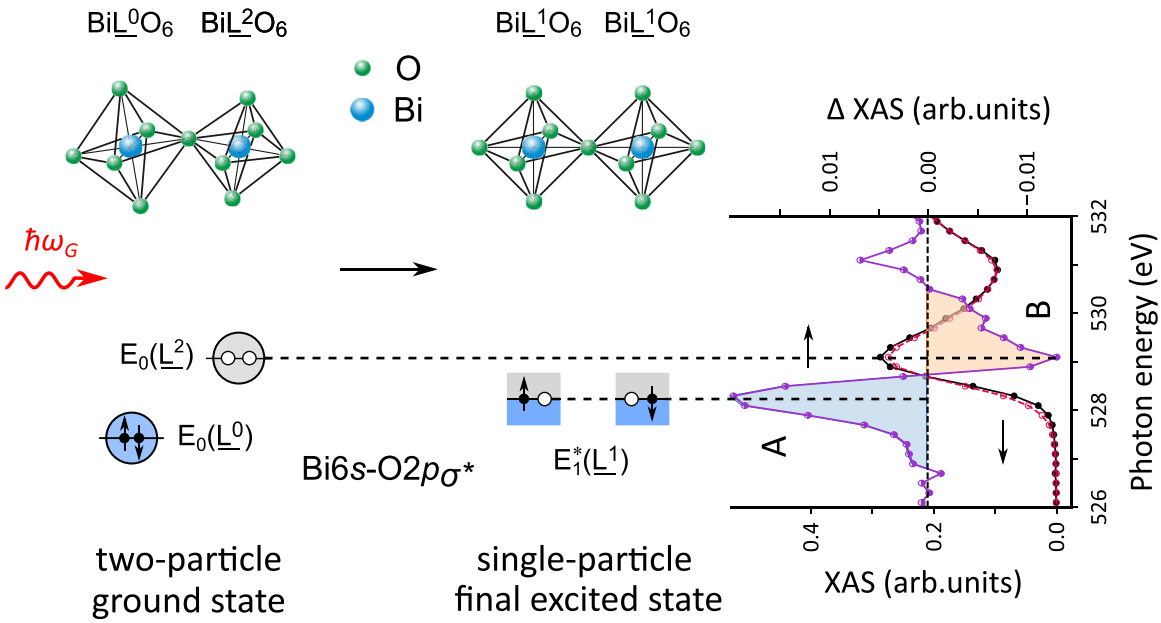

FIG. 5. Scheme of $BaBiO_3$ ground state excitation by a resonant optical photon. The main changes occur in $BaBiO_3$ upon the fast resonant excitation over the optical gap. The simultaneous rearrangement of local electronic (bottom panel) and local crystal (top panel) structures is reflected in the shape of the O *K*-edge XAS and the difference spectrum ΔXAS of $BaBiO_3$ at the delay time 0.8 ps (right panel).

small octahedral complexes, respectively. Based on the general assumptions about such conditions, which we describe below in detail, the features of the difference spectra in the preedge region of XAS can be associated with the contributions from the paired and single electron and hole states before and after the excitation.

As we showed in the previous section, the energy position of peak A [Figs. 2(b), 2(c) and 2(d)] in the difference spectrum is stabilized at the delay time 0.8 ps after the arrival of the laser pulse. This suggests that the process of both local electronic and crystal structure rearrangement in $BaBiO_3$ is nearly complete by this time. Therefore, we will start the analysis of difference spectrum from the delay time 0.8 ps when the final excited state is achieved. The fast transients occurring at the delay times 0–0.8 ps will be discussed in detail later.

In the ground state of $BaBiO_3$ (Fig. 5) the alternating large $Bi\underline{L}^0O_6$ and small $Bi\underline{L}^2O_6$ octahedral complexes carry the local pair of electrons (blue) and holes (gray) on the upper antibonding Bi 6*s*–O $2p_{\sigma^*}$ orbital, respectively. The absorption of a short laser pulse with photon energy resonant with the optical gap $\hbar\omega_G = E_G$ leads to the destruction of local electron and hole pairs. Thus the two-particle local electronic structure with pair states $E_0(\underline{L}^0)$ and $E_0(\underline{L}^2)$ transforms into the single-particle local electronic structure with two similar $E_1^*(\underline{L}^1)$ states containing one electron and one hole at the final stage of excitation. Two single electrons from the broken pair are excited by ∼1 eV to the $E_1^*(\underline{L}^1)$ energy level. At the same time two single holes $\underline{L}^1$ from the broken hole pair appear on the same $E_1^*(\underline{L}^1)$ level approximately 1 eV lower than the paired holes state $E_0(\underline{L}^2)$.

Such a local electronic structure transformation induces a lattice rearrangement from the monoclinic structure with different $Bi\underline{L}^0O_6$ and $Bi\underline{L}^2O_6$ octahedra to the cubic structure with similar octahedra $Bi\underline{L}^1O_6$, each of them containing one electron and one hole on the upper antibonding Bi 6*s*–O $2p_{\sigma^*}$ orbital.

These changes can be associated with the features observed in the preedge region of difference spectrum ΔXAS (Fig. 5) at the delay time $\geqslant 0.8$ ps after the laser excitation. The positive peak A in ΔXAS at lower photon energy we attribute to the appearance of single unpaired holes $\underline{L}^1$ at the energy level $E_1^*(\underline{L}^1)$, resulting from the local pair dissociation at the final stage of excitation. The negative peak B in ΔXAS at higher photon energy we attribute to the reduction of formerly unoccupied states due to the decrease of the number of paired holes $\underline{L}^2$ at the energy level $E_0(\underline{L}^2)$.

It is important to emphasize that, although the excitation photon energy is $\hbar\omega_G \approx 2$ eV, the separation between the peaks A and B in the difference spectrum ΔXAS is clearly ∼1 eV. We interpret this as a fingerprint of the transition from a two-particle to a single-particle spectrum, caused by the resonant optical excitation. In this case the quantum energy $\hbar\omega_G \approx 2$ eV, required to break one local electron pair, is split between two resulting single electrons, which are excited each by ∼1 eV to the new level $E_1^*(\underline{L}^1)$. Indeed, if we assume that two electrons at the $E_0(\underline{L}^0)$ level are not bound into a local pair, but the ground state represents a single-electron spectrum, then the shape of ΔXAS upon resonant excitation through the semiconductorlike CDW gap would be different. In that case, a quantum $\hbar\omega_G \approx 2$ eV would excite one of the two single electrons from the ground level $E_0(\underline{L}^0)$ to a vacant state in the preedge region and a hole would appear at the level $E_0(\underline{L}^0)$. As a result, the peaks A and B would also be observed in the ΔXAS spectrum, but the separation between them would be ∼2 eV, which is not what we observed.

Thus the effects observed in the preedge region of O *K*-edge XAS upon resonant optical excitation should be considered as the direct experimental evidence that $BaBiO_3$

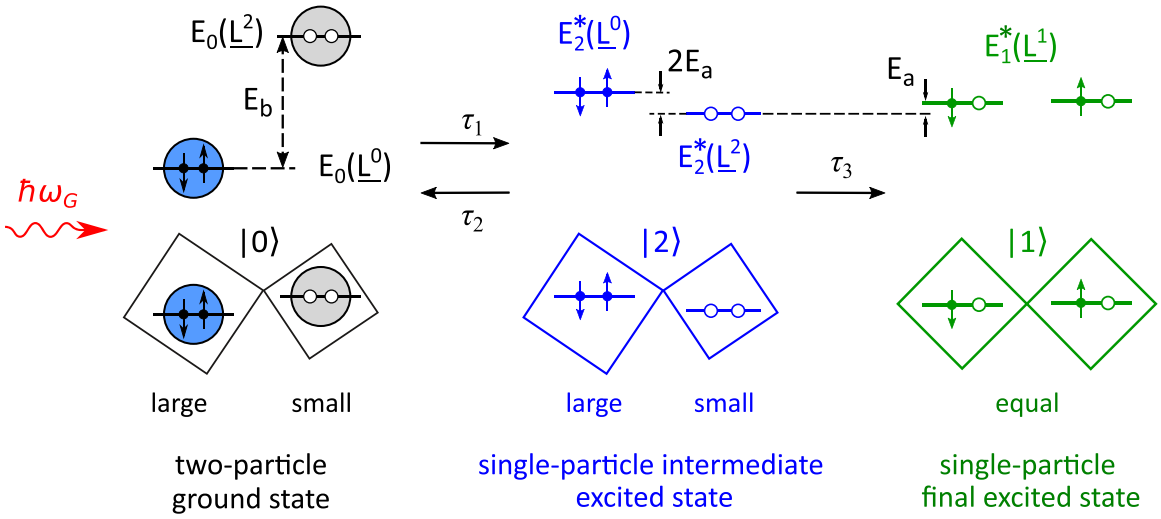

FIG. 6. Scheme of fast transients occurring in $BaBiO_3$ at short delay times after excitation. The detailed scheme of $BaBiO_3$ local electronic structure (top) and local crystal structure (bottom) rearrangement observed at the delay times 0–0.8 ps after femtosecond resonant excitation over the optical gap $\hbar\omega_G = E_G$. Left panel: the two-particle paired ground state $E_0(\underline{L}^0) + E_0(\underline{L}^2)$; middle panel: the single-particle unpaired intermediate excited state $E_2^*(\underline{L}^0) + E_2^*(\underline{L}^2)$; right panel: the single-particle metastable final excited state $2E_1^*(\underline{L}^1)$.

is a unique compound with initially paired carriers forming a new quantum state of the local pair density wave (LPDW).

In the model [39,48,49], the local electron and hole pairs in the neighboring octahedra are directly linked. The presence of an electron pair at the energy level $E_0(\underline{L}^0)$ in the large octahedron assumes the presence of the hole pair $\underline{L}^2$ at the energy level $E_0(\underline{L}^2)$ in the nearest small octahedron. The configuration of the ground state local electronic structure of $BaBiO_3$ should then be understood as $E_0(\underline{L}^0) + E_0(\underline{L}^2)$ (Fig. 5). Different occupation ($\underline{L}^2$ or $\underline{L}^0$) of the antibonding Bi $6s-$O $2p_{\sigma^*}$ orbital defines the configuration and the size of octahedron and is the primary cause for the lattice breathing and tilting distortions, but not vice versa. In the case of equal occupation $\underline{L}^1$ of the antibonding Bi $6s-$O $2p_{\sigma^*}$ orbital in the nearest octahedra no breathing distortion can happen and the structure should consist of identical $Bi\underline{L}^1O_6$ octahedra (Fig. 5).

Figures 2(c) and 2(d) show the dynamics of shape and energy position of peak A (appearance and growth of the unpaired holes) in the difference spectra ΔXAS for the delay times 0.1, 0.2, 0.3, 0.5, 0.8, and 1.8 ps. However, the little precursors of the peaks A and B are observed in ΔXAS already at time zero (the maximum overlap between the pump and probe pulses) and the separation between them is ∼1 eV [Fig. 2(b)]. It means that the process of local pair dissociation after the absorption of the optical photon begins within the time resolution of our experiment (a few tens of fs). At the delay time 0.1 ps after the excitation the peaks A and B already have significant amplitudes which keep growing further. During the delay time 0.1–0.8 ps the peak A shifts slightly to the higher energy by ∼0.2 eV, while its amplitude reaches the maximum near the delay time 0.2 ps. Between ∼0.5 and 0.8 ps the position of peak A stabilizes and does not change at further delay times [Fig. 2(d)].

The transition processes occurring in the local electronic and crystal structure of $BaBiO_3$ at the early times from 0 to 0.8 ps after the resonant laser excitation over the optical gap are summarized schematically in Fig. 6.

As mentioned before, the ground state is observed in the O K-edge XAS spectrum of unexcited $BaBiO_3$ [Fig. 2(b); Fig. 5] as a preedge peak at an energy corresponding to the unoccupied level $E_0(\underline{L}^2)$ in the Bi $6s-$O $2p_{\sigma^*}$ orbital of the small $Bi\underline{L}^2O_6$ complex. The energy level $E_0(\underline{L}^0)$ occupied by the electron pair in the large $Bi\underline{L}^0O_6$ octahedron in the ground state $|0\rangle$ (Fig. 6, left panel) does not appear in XAS, because it lacks the density of unoccupied states $\underline{L}^0$, while XAS is sensitive only to the vacant states.

In order to describe the transition processes taking place during the short delay times 0–0.8 ps in Fig. 6 we use the expression for the pairing (pair bonding) energy E_b [42,43,48,49]:

$$E_b = E(Bi\underline{L}^1O_6 + Bi\underline{L}^1O_6) - E(Bi\underline{L}^0O_6 + Bi\underline{L}^2O_6) = E_G - 2E_a, \quad (2)$$

where $E_G = \hbar\omega_G$ is the optical gap and $2E_a$ is the activation gap.

In the two-particle spectrum of the $BaBiO_3$ ground state, $|0\rangle$, the electron and hole pairs are combined with pair binding energy E_b, so that the energy separation between levels $E_0(\underline{L}^2)$ and $E_0(\underline{L}^0)$ is equal to $E_b = E_G - 2E_a$ (Fig. 6, left panel).

The first stage of excitation after the absorption of resonant ($\hbar\omega_G = E_G \approx 2$ eV) optical pump pulse at the delay times 0–0.3 ps corresponds to the transformation from a two-particle (Fig. 6, left panel) to a single-particle spectrum (Fig. 6, middle panel). At this stage the following processes with characteristic time τ_1 occur (Fig. 6, middle panel): both local electron and hole pairs dissociate simultaneously according to the optical transition $E_0(\underline{L}^0) + E_0(\underline{L}^2) \xrightarrow{\hbar\omega_G} E_2^*(\underline{L}^0) + E_2^*(\underline{L}^2)$. It transforms the two-particle energy structure to the new single-particle one and $E_2^*(\underline{L}^0)$ and $E_2^*(\underline{L}^2)$ are the intermediate excited single-electron and single-hole levels with two unpaired electrons and two unpaired holes in the large and

small octahedra, respectively, in the intermediate excited state $|2\rangle$. So, the energy of both electrons increases by $\hbar\omega_G/2 = E_b/2 + E_a \approx 1$ eV relative to the initial $E_0(\underline{L}^0)$ level, while the energy of the $E_2^*(\underline{L}^2)$ level with two unpaired holes shifts by the same value $\hbar\omega_G/2$ in the opposite direction relative to the initial $E_0(\underline{L}^2)$ position. The activation gap $2E_a$ appears between the levels $E_2^*(\underline{L}^0)$ and $E_2^*(\underline{L}^2)$. Note that, at the first stage of excitation, the two unpaired electrons and two unpaired holes remain in their own octahedra, thus maintaining the breathing distortion of the lattice due to different occupation ($\underline{L}^2$ and $\underline{L}^0$) of the antibonding Bi $6s$−O $2p_{\sigma^*}$ orbital.

While the lattice is not rearranged yet, the intermediate excited state $|2\rangle$ can relax back to the ground state. This process with characteristic time τ_2 happens as a reverse transition $E_2^*(\underline{L}^0) + E_2^*(\underline{L}^2) \rightarrow E_0(\underline{L}^0) + E_0(\underline{L}^2)$, which is probably accompanied by the emission of a photon with an energy $\hbar\omega \sim 2$ eV, giving back the pairing energy E_b.

The first stage of excitation with characteristic time τ_1 is observed in the difference spectrum ΔXAS [Figs. 2(b) and 2(c)] at the delay times 0–0.3 ps as the simultaneous appearance and growth of peak A [appearance and increase of the number of unpaired holes at the level $E_2^*(\underline{L}^2)$] and negative peak B [decrease of the number of paired holes at the level $E_0(\underline{L}^2)$], proportional to the number of broken pairs. The process of recombination to the initial paired state with characteristic time τ_2 becomes noticeable after ∼0.2 ps only as a slight decrease of the peak A and B amplitudes.

At delay times 0.3–0.8 ps after the initial excitation the dominant process is the transformation of the local electronic structure with levels $E_2^*(\underline{L}^0)$ and $E_2^*(\underline{L}^2)$, belonging to the different octahedra, and occupied by two unpaired electrons and two unpaired holes, respectively, into the structure with two half-filled $E_1^*(\underline{L}^1)$ levels, corresponding to the identical octahedra (the final excited state $|1\rangle$). This transition, described by equation $E_2^*(\underline{L}^0) + E_2^*(\underline{L}^2) \rightarrow 2E_1^*(\underline{L}^1)$, leads to the rearrangement of the lattice into a cubic structure with identical octahedra. This process is accompanied by the closing of the activation gap $2E_a$ and characterized by the time τ_3 (see Fig. 6, right panel).

In the ΔXAS spectrum this stage at the delay times 0.3–0.8 ps must be observed as the shift of peak A to higher energy by the value of E_a due to the transformation of the $E_2^*(\underline{L}^2)$ level to the $E_1^*(\underline{L}^1)$ levels. Indeed, taking $E_a \approx 0.24$ eV from [17] we obtain an exhaustive explanation of the peak A shift by ∼0.2 eV, observed in the difference spectrum ΔXAS [see Figs. 2(c) and 2(d)].

After the final state of excitation is reached, the electronic transition $2E_1^*(\underline{L}^1) \rightarrow E_0(\underline{L}^0) + E_0(\underline{L}^2)$ back to the ground state $|1\rangle \rightarrow |0\rangle$ is forbidden, since it requires the energy E_a for the reverse rearrangement of the lattice. Thus, in the final state $|1\rangle$, the system has the structure of identical octahedra with a half-filled antibonding Bi $6s$−O $2p_{\sigma^*}$ orbital and it is metastable until at least 60 ps.

The slow monotonous decrease of the peak amplitudes in the difference spectrum at large delay times 0.8–60 ps [Fig. 2(b)] indicates that the excited state of the system still tends to relax to the ground state in a very long time compared to the time scale of our experiment. This relaxation happens probably due to the interaction of initially optically excited volume with a surrounding unexcited matrix. Note that the fraction of the excited state in the probed volume does not exceed 5% at the pump fluence of 8 mJ/cm^2 (Fig. 3).

Taking into account the fitting of the difference spectrum ΔXAS at the energy of peak A using the three-exponential model (Fig. 4) and the fast transients observed at the delay times 0–0.8 ps (Fig. 6), we can estimate the characteristic time of local electron and hole pairs destruction by the resonant femtosecond excitation over the optical gap as $\tau_1 = 0.15$ ps, the time of pairs recombination (relaxation to the ground paired state) as $\tau_2 = 0.24$ ps, and the time of rearrangement of the lattice into a new cubic structure with identical octahedra as $\tau_3 = 1.5$ ps. Similar characteristic times were also obtained from the three-exponential fit of the spectrum at the energy of negative peak B (Fig. S2 in the Supplemental Material [57]). It is quite natural since the dynamics of both peaks A and B is defined by the same process of local pair dissociation.

The relatively large characteristic time at the first stage of excitation, estimated as $\tau_1 \sim 0.15$ ps (Fig. 4), can be considered as another argument in favor of the $BaBiO_3$ two-particle ground state. Indeed, in the case of a single-particle state, the excitation time of a single electron upon the absorption of a $\hbar\omega_G \approx 2$ eV photon is expected to be of the femtosecond time scale and therefore should be observed in the spectrum as faster process closer to the laser pulse duration. Apparently, the dissociation of a paired state is a process more complicated than the excitation of a single electron and requires the additional energy and time cost.

The first direct observation of fast processes of electron and hole pair dissociation accompanied by lattice rearrangement at the short delay times of 0–0.8 ps (Fig. 6) is another very important fundamental result of this work. It demonstrates directly the nature of the two gaps in $BaBiO_3$ and indicates that, upon femtosecond resonant optical excitation, the carrier pairing and bond disproportionation disappear and optical and activation gaps close. The latter is the sign of the insulator-metal phase transition, so in the excited state the system with a cubic structure and identical octahedra should exhibit metallic properties, which agrees well with the results of our DFT calculations [58,59]. Therefore, $BaBiO_3$ in the metastable excited state behaves as the imaginary system $BaBi^{4+}O_3$ [18,60], a metal with a half-filled band.

In addition, it is worth noting that the density of states of paired local ligand holes $E_0(\underline{L}^2)$ in the two-particle spectrum (Fig. 6, left panel) which appears in the ground state XAS as the preedge peak [Fig. 2(b)], upon resonant excitation over the optical gap transforms into the density of vacant single states $E_1^*(\underline{L}^1)$ in the single-particle spectrum (Fig. 6, right panel) and forms a conduction band in a metallic metastable excited state.

The existence of two energy gaps in $BaBiO_3$ was previously proposed in a number of works [17,31,32,42], but here we directly evidence that the optical gap is related to the pairing energy and the activation gap as $E_G = E_b + 2E_a$. The pairing energy E_b is responsible for binding the electrons and the holes located on completely filled and unoccupied levels in the large and small octahedra, respectively. The activation energy E_a is related to the breathing-type deformation of the cubic structure and the formation of the structure with different octahedra (Fig. 6). It is the pairing energy E_b that ensures the energy gain and makes the bond

disproportionation process in $BaBiO_3$ energetically favorable. The activation gap E_a represents an energy barrier in the two-particle spectrum that prevents two-particle charge transfer in the structure with different octahedra and disappears upon the lattice rearrangement into a system with identical octahedra at the insulator-metal transition. As was pointed out earlier, in the two-particle charge transfer the activation gap plays a role of the pair localization energy [39,48,49].

The extraordinarily large value of the preexponential factor in the transport measurements $n(T) = n_0 \exp(-E_a/kT)$, where $n_0 = 1.1 \times 10^{22}$ cm^{-3} is equal to the number of unit cells [17], becomes obvious since we have shown that every unit cell in $BaBiO_3$ carries a local pair and participates in the two-particle conductivity.

In addition, the nature of the extremely large amplitude of the breathing mode at ~570 cm^{-1} in the Raman spectra [17,61] upon resonant excitation over the optical gap is clarified. The breaking of the carrier pairs leads to fast (0.8 ps) local structure rearrangement and the closing of the activation gap. The released energy brings about an abnormal increase in the intensity of the breathing mode together with its higher harmonics up to the fourth order in Raman spectra [17,61].

It is worth noting that the analysis of fast transients at the delay times 0–0.8 ps gives the new important experimental insight into the bond disproportionation mechanism in $BaBiO_3$. This casts doubt on the conclusions previously obtained from the DFT calculations that the breathing mode or the different local environments of the Bi atom in $BaBiO_3$ are responsible for the bond disproportionation [28,29]. Our experiment shows that the local electronic and crystal structure of the final excited state (Fig. 6, right panel), that corresponds to the cubic lattice of imaginary system $BaBi^{4+}O_3$, cannot be transformed into a breathing distorted structure with large and small octahedra (Fig. 6, middle panel) by the simple transition of one of the ligand holes $\underline{L}^1$ to the neighboring octahedron ($\underline{L}^1 \rightarrow \underline{L}^2$) because it requires an energy cost of E_a. Such a transition is energetically favorable only if two electrons and two holes form local pairs in the large and small octahedra, respectively, releasing the binding energy E_b (Fig. 6, left panel). Thus the mechanism of bond disproportionation in the $BaBiO_3$ ground state can be realized only due to the local pairing of electrons and holes in real space.

Introducing the concept of local pair density wave (LPDW) as a new quantum state of charge carriers in $BaBiO_3$, we use the local nature of the charge density wave (CDW) [20,30], but emphasize the importance of carrier pairing and the strong localization of electron and hole pairs in real space on the different octahedra of the crystal structure. In the case of an ordinary CDW, the charge carriers do not have to be in a paired state, while the LPDW is formed by the alternating local electron and hole pairs in the neighboring octahedra. Besides, such a definition shows the difference between such a local pair density wave and the PDW state recently discovered in cuprate HTSCs [62]. Indeed, the PDW in cuprates describes a wave of carriers paired in reciprocal space, while the LPDW is strictly related to the local pairing of electrons and holes in real space. Moreover, the LPDW state has a dynamic character due to the local pair tunneling between the neighboring complexes in accordance with the dynamic exchange $Bi\underline{L}^2O_6 \leftrightarrow Bi\underline{L}^0O_6$, causing oxygen atom oscillations in a double-well potential [39]. The LPDW state with alternating local electron and hole pairs means that the charge difference between the neighboring octahedra is exactly $2e$.

A similar real-space pairing phenomenon was previously discussed in cuprate HTSCs, $SrTiO_3$, and related compounds with a perovskitelike structure as the appearance of a prepairing preceding the formation of a superconducting state [63–65]. For example, in the Zr-doped $SrTiO_3$, where the existence of unconventional real space pairing was predicted in [66], the preformed electron pairs can be considered as a precursor of the superconducting Bose-Einstein condensate (BEC) at lower temperatures and lower magnetic fields. In the BEC regime, pairing has a local nature and precedes the formation of a superconducting state [65].

Our results also allow for a deeper understanding of the local processes occurring in $BaBiO_3$ with potassium doping, described earlier in the model of spatially separated Fermi-Bose mixture, which explains the microscopic mechanism of superconductivity in bismuthates [48,49]. Replacing every two barium atoms with two potassium atoms adds two holes and replaces the part of large $Bi\underline{L}^0O_6$ octahedra with small $Bi\underline{L}^2O_6$ ones. However, these additional holes are in the unpaired state as in the middle panel of Fig. 6, since there are no large octahedra $Bi\underline{L}^0O_6$ with paired electrons nearby. We could guess that the emergence of these new unpaired states was observed in [24,33,56] in the O K-edge XAS spectrum of $Ba_{1-x}K_xBiO_3$ as a shift of the preedge peak to lower energy by ~1 eV. It coincides with the position of the unpaired hole level in the difference spectrum of the excited state $E_1^*(\underline{L}^1)$ of $BaBiO_3$ upon resonant laser excitation [Figs. 2(b) and 5] observed in this work.

The growing number of small octahedra with doping leads to their intersection in real space, causing the splitting of their unoccupied levels. When the percolation limit $x = 0.37$ is reached and exceeded, these levels merge into the conduction band [39,67], providing an insulator-metal phase transition in the fermionic subsystem, similar to the metastable metallic excited state of $BaBiO_3$ (Fig. 6, right panel).

At the same time, the local electron pairs in the $Bi\underline{L}^0O_6$ octahedra, representing the bosonic subsystem, do not disappear with doping and can travel freely along the [100]-type axes, providing superconductivity at $x \geqslant 0.37$ [39,48,49].

New arguments are also given in order to explain the splitting of Bi $4f$ lines in superconducting $Ba_{1-x}K_xBiO_3$, discovered in x-ray photoemission spectroscopy (XPS) experiments [23,24,68,69]. These observations, in our opinion, play an essential role in understanding the mechanism of superconductivity in bismuthates. Our results suggest that the ground state of $BaBiO_3$ (Fig. 6, left panel) can be considered as a two-particle (bosonic) analog of a conventional semiconductor with a band gap E_b and the bosonic chemical potential μ_0 in the center of this band. This μ_0 level is common for all octahedra, which defines the absence of splitting of the Bi $4f$ states counted from μ_0 and indicates the same valence state of all bismuth ions in $BaBiO_3$ [23–25,68]. In superconducting $Ba_{1-x}K_xBiO_3$, the local electron and hole pairs are stored in the bosonic subsystem with their own chemical potential μ_0. At the same time, with $x \geqslant 0.37$ the additional unpaired holes in small octahedra form a conduction band in the fermionic subsystem with fermionic chemical potential μ_F at the energy

position $E_0(\underline{L}^0)$. Since the fermionic and bosonic subsystems are spatially separated (i.e., they belong to different octahedra) [48,49], the binding energies of Bi $4f$ states counted from two different chemical potentials are separated as well. It results in their splitting and the occurrence of two bismuth valence states in superconducting $Ba_{1-x}K_xBiO_3$.

Our observation of a quantum LPDW state in bismuthates has something in common with the recent insight into the high-temperature superconductivity mechanism in cuprates, proposed in [70,71]. The authors studied how the quantum phase coherence evolves across the superconductor-metal-insulator transition by looking at the quantum magnetoconductance $\hbar/2e$ oscillations in the anomalous bosonic metallic state in nanopatterned $YBa_2Cu_3O_{7-\delta}$, which is similar to the Fermi-Bose mixture in the metallic superconducting $Ba_{1-x}K_xBiO_3$ [48,49].

Taking into account a large number of similarities between bismuthate and cuprate HTSCs [44,72], including the strong anharmonicity due to the oxygen atom vibrations in a double well potential [73–77], the transition to a synchronized phase in the charge-lattice dynamics [76,78], the coexistence of the small bosonic and fermionic charge carriers [79], observation of the preformed pairing [63,65], and the behavior of electronic structure in the time-resolved experiments [52,53,80], we hope to extend our model [48,49] to the cuprates as well [75,81]. Thus we expect that the results of our experiment will give a new impetus to the development of a unified model of high-temperature superconductivity in all superconducting oxides with a perovskitelike structure.

IV. CONCLUSIONS

Our time-resolved XAS experiment on $BaBiO_3$ with a femtosecond resonant laser excitation through the optical gap shows evidence of local electron and hole pairs existing in the ground state of $BaBiO_3$.

The changes observed in XAS at the short delay times from 0 to 0.8 ps allowed us to extract the characteristic times of local pair dissociation ($\tau_1 = 0.15$ ps), of pair recombination ($\tau_2 = 0.24$ ps), and of the lattice rearrangement from the monoclinic structure with breathing and tilting distortions into the cubic structure with identical octahedra ($\tau_3 = 1.5$ ps). This helped us to elucidate the intermediate phase of excitation and to explain the mechanism of bond disproportionation in $BaBiO_3$.

We see that after the excitation the system does not relax into the initial state for at least 60 ps (the maximum delay time in our experiment). Instead, it remains in the new quasiequilibrium state with the structure of identical octahedra. Since both the optical and activation gaps close shortly after the excitation, this metastable state probably behaves as a metal with a half-filled valence band.

In summary, the changes in the XAS spectrum of $BaBiO_3$ at short delay times after the excitation can hardly be explained using the single-electron approach, but can be interpreted much more consistently as a trace of broken charge carrier pairs. It suggests that the ground state of $BaBiO_3$ is not a conventional CDW, but the new quantum state of local pair density wave (LPDW).

ACKNOWLEDGMENTS

We acknowledge European XFEL in Schenefeld, Germany, for provision of x-ray free-electron laser beamtime at Scientific Instrument SCS and thank the instrument group and facility staff for their assistance. A.P.M., A.I., V.N., A.L., A.K., A.A.Y., I.K., A.V.K., V.P., and O.K. acknowledge the Ministry of Science and Higher Education of the Russian Federation (Agreement No. 075-15-2021-1352) for the financial support. The calculations were performed with the support of the MEPhI Program Priority 2030.

APPENDIX A: SAMPLE PREPARATION AND CHARACTERIZATION

We prepared 90-nm-thick films of $BaBiO_3$ on Si(100) substrates using pulsed laser deposition in the oxidizing atmosphere of N_2O. During deposition the temperature of the substrate was maintained at 500 °C and the pressure of N_2O at 50 mTorr. A polycrystalline $BaBiO_3$ target was synthesized by the standard solid phase reaction from a stoichiometric mixture of Bi_2O_3 and $BaCO_3$ powders. The mixture was annealed at 800 °C in three sessions, 8 h each, with intermediate grinding of the powder in an agate mortar. Then, the obtained powder was pressed into a tablet and sintered at 850 °C for 12 h. To ablate the target we used the excimer KrF laser, operating at $\lambda = 248$ nm, the repetition rate 10 Hz, pulse energy 100 mJ, and the fluence 1.6 J/cm^2 at the target surface. In order to eliminate the macrosized particles in the ablated flux we implemented a direct flux screening approach when the substrate is placed behind the screen in its shadow and the film grows from a highly dispersed fraction of the flux, scattered on the molecules of the ambient gas in the deposition chamber. The Si(100) substrate (Silson Ltd.) was a single-crystal plate of 7.5×7.5 mm^2 with alternating rows of etched windows with Si(100) membranes and empty apertures of the size 0.2×0.2 mm^2. The Si(100) membrane thickness was 100 nm. The film thickness was evaluated by stylus profilometry of the reference samples using the Dektak 150 stylus profiler. The films were characterized by XRD (Rigaku Ultima IV, Cu K_α), scanning electron microscopy (Tescan VEGA3 SB), and Raman spectroscopy (LabRAM HR Evolution Raman spectrometer, He-Ne laser, $\lambda = 633$ nm). The XRD analysis of the reference samples revealed 98% of the polycrystalline monoclinic phase with space group $I12/m1$ in the films. Raman spectra demonstrated a strong peak at 563 cm^{-1} corresponding to the breathing mode of $BaBiO_3$. More data on the sample characterization is given in Supplemental Material [57].

APPENDIX B: TIME-RESOLVED XAS EXPERIMENT

The time-resolved x-ray absorption spectroscopy experiment was performed at the SCS instrument of European XFEL. The photon energy was scanned in the range 525–550 eV across the O K absorption edge, using the synchronized motion of the monochromator grating and the undulator gap. In first order diffraction the soft x-ray monochromator provides an x-ray bandwidth of 100 meV in this photon energy range [55]. The array of $BaBiO_3$ samples

was installed on a sample holder that could be moved in three spatial directions relative to the beam.

For the XAS measurement, we used the novel technique comprising the beam splitting off-axis zone plate [54] combined with the pulse-resolved DSSC detector [82]. In this scheme, the incident x-ray beam is split by the zone plate in three diffraction orders [Fig. 2(a)]. Two of the resulting beams pass through the sample array windows containing $BaBiO_3$, one of which is pumped by the optical laser, while the third beam passes through the empty aperture. The beams produce three spots on a single module of the DSSC detector. By integrating over these spots we obtain the values for the pumped, unpumped, and reference x-ray pulse intensity. Such a technique significantly improves the accuracy which is crucial for the transient XAS measurement at the x-ray free electron laser. In this work we used this scheme slightly modified: the optical laser pulse was arriving on the sample window with half of the x-ray pulse repetition rate. Thus the pumped and unpumped x-ray intensities for the analysis were obtained from the same window, which eliminates the possible problem of sample inhomogeneity. The x-ray beam was collimated on the zone plate using a Kirkpatrick-Baez mirror system. After the zone plate, the beams were diverging, resulting in the x-ray spot size on the sample ∼50 μm and the x-ray fluence ∼0.2 mJ/cm^2.

The sample was pumped by 50 fs optical pulses of the photon energy 1.96 eV (the wavelength 633 nm), which corresponds to the optical gap in the thin film $BaBiO_3$ [83]. The pump pulses were produced by a tunable optical parametric amplifier driven by the femtosecond SASE3 pp-laser with a fundamental wavelength 800 nm. The spatial overlap between the x-ray and laser beams was verified by microscope camera images. The temporal overlap was verified in two stages. Coarse timing was done using the overlap of x-ray and laser signals measured by an antenna connected to a fast oscilloscope. Fine timing was achieved by measuring the x-ray pump-optical probe reflectivity from a silicon nitride membrane, installed on the sample holder in the same plane as the $BaBiO_3$ sample. The laser spot size on the sample was 150 μm and the optical fluence was increased up to 32 mJ/cm^2. However, the majority of XAS spectra were measured with the optical pump fluence 8 mJ/cm^2 to avoid sample damage. The time resolution of the pump-probe experiment was ∼70 fs. Experiments were performed at a 10 Hz repetition rate using one x-ray pulse to probe the initial state of the sample and another x-ray pulse, arriving approximately 140 μs later, to probe the sample excited by the optical pump pulse. The delay time between the optical pump and the x-ray probe pulse varied from −1 to 60 ps.

APPENDIX C: *AB INITIO* CALCULATIONS

Ab initio calculations were performed using the full-potential linearized augmented plane wave (FP-LAPW) method implemented in the WIEN2K software package [84]; to include the exchange-correlation potential in our calculations, we utilized the Perdew-Burke-Ernzerhof (PBE) gradient correction method. We employed a resolution of 400 **k** points in the first Brillouin zone. The crystal structure for the ground state was taken from [85]. The structure of the system is characterized by different lengths of Bi-O bonds, which are determined by the occupancy of the antibonding Bi $6s-O\ 2p_{\sigma^*}$ orbital. The ground state exhibits insulating behavior, with an indirect gap of 0.3 eV and a direct gap of less than 2 eV. In the excited state, the material adopts a simple cubic structure with the length of the Bi-O bond equal to the average size of the initial octahedra.

[1] R. L. Bouwmeester and A. Brinkman, $BaBiO_3$-From single crystals towards oxide topological insulators, Rev. Phys. **6**, 100056 (2021).

[2] R. L. Bouwmeester, A. Brinkman, and K. Sotthewes, Thickness-dependent band gap modification in $BaBiO_3$, Nanomaterials **11**, 882 (2021).

[3] H. Cao, H. Guo, Y.-C. Shao, Q. Liu, X. Feng, Q. Lu, Z. Wang, A. Zhao, A. Fujimori, Y.-D. Chuang, H. Zhou, and X. Zhai, Realization of electron antidoping by modulating the breathing distortion in $BaBiO_3$, Nano Lett. **21**, 3981 (2021).

[4] R. Kashikar and B. R. K. Nanda, Feeble metallicity and robust semiconducting regime in structurally sensitive Ba(Pb, Sn)O_3 alloys, Appl. Phys. Lett. **119**, 152103 (2021).

[5] B. Yan, M. Jansen, and C. Felser, A large-energy-gap oxide topological insulator based on the superconductor $BaBiO_3$, Nat. Phys. **9**, 709 (2013).

[6] S. Griffitt, M. Spaić, J. Joe, Z. W. Anderson, D. Zhai, M. J. Krogstad, R. Osborn, D. Pelc, and M. Greven, Local inversion-symmetry breaking in a bismuthate high-T_C superconductor, Nat. Commun. **14**, 845 (2023).

[7] M. Talha and Y. W. Lee, Raman modes and dielectric relaxation properties of epitaxial $BaBiO_3$ thin films, Mater. Res. Express **7**, 016420 (2020).

[8] N. Feng, J. Han, C. Lin, Z. Ai, C. Lan, K. Bi, Y. Lin, K.-H. Xue, and B. Xu, Anti-Jahn-Teller effect induced ultrafast insulator to metal transition in perovskite $BaBiO_3$, npj Comput. Mater. **8**, 226 (2022).

[9] Q. Zhao, T. Abe, C. Moriyoshi, S. Kim, A. Taguchi, H. Moriwake, H.-T. Sun, and Y. Kuroiwa, Charge order of bismuth ions and nature of chemical bonds in double perovskite-type oxide $BaBiO_3$ visualized by synchrotron radiation x-ray diffraction, Jpn. J. Appl. Phys. **59**, 095505 (2020).

[10] R. L. Bouwmeester, T. Jansen, M. Altena, G. Koster, and A. Brinkman, Observing structural distortions in complex oxides by x-ray photoelectron diffraction, J. Electron Spectrosc. Relat. Phenom. **257**, 147201 (2022).

[11] Y.-C. Yam, M. M. Moeller, G. A. Sawatzky, and M. Berciu, Peierls versus Holstein models for describing electron-phonon coupling in perovskites, Phys. Rev. B **102**, 235145 (2020).

[12] M. R. Benam, K. Foyevtsova, A. Khazraie, I. Elfimov, and G. A. Sawatzky, Bond versus charge disproportionation and nature of the holes in *s-p* ABX_3 perovskites, Phys. Rev. B **104**, 195141 (2021).

[13] S. Sarkar, R. Raghunathan, S. Chowdhury, R. J. Choudhary, and D. M. Phase, The mystery behind dynamic charge disproportionation in $BaBiO_3$, Nano Lett. **21**, 8433 (2021).

[14] A. Sleight, J. Gillson, and P. Bierstedt, High-temperature superconductivity in the $BaPb_{1-x}Bi_xO_3$ systems, Solid State Commun. **17**, 27 (1975).

[15] L. F. Mattheiss, E. M. Gyorgy, and D. W. Johnson, Superconductivity above 20 K in the Ba-K-Bi-O system, Phys. Rev. B **37**, 3745 (1988).

[16] H. Sato, S. Tajima, H. Takagi, and S. Uchida, Optical study of the metal-insulator transition on $Ba_{1-x}K_xBiO_3$ thin films, Nature (London) **338**, 241 (1989).

[17] S. Uchida, K. Kitazawa, and S. Tanaka, Superconductivity and metal-semiconductor transition in $BaPb_{1-x}Bi_xO_3$, Phase Transit. **8**, 95 (1987).

[18] D. Cox and A. Sleight, Crystal structure of $Ba_2Bi^{3+}Bi^{5+}O_6$, Solid State Commun. **19**, 969 (1976).

[19] D. E. Cox and A. W. Sleight, Mixad-valent $Ba_2Bi^{3+}Bi^{5+}O_6$: Structure and properties *vs* temperature, Acta Crystallogr. Sect. B **35**, 1 (1979).

[20] T. M. Rice and L. Sneddon, Real-space and k-space electron pairing in $BaPb_{1-x}Bi_xO_3$, Phys. Rev. Lett. **47**, 689 (1981).

[21] C. Franchini, G. Kresse, and R. Podloucky, Polaronic hole trapping in doped $BaBiO_3$, Phys. Rev. Lett. **102**, 256402 (2009).

[22] C. Franchini, A. Sanna, M. Marsman, and G. Kresse, Structural, vibrational, and quasiparticle properties of the Peierls semiconductor $BaBiO_3$: A hybrid functional and self-consistent GW+vertex-corrections study, Phys. Rev. B **81**, 085213 (2010).

[23] G. K. Wertheim, J. P. Remeika, and D. N. E. Buchanan, Electronic structure of $BaPb_{1-x}Bi_xO_3$, Phys. Rev. B **26**, 2120 (1982).

[24] M. Qvarford, V. G. Nazin, A. A. Zakharov, M. N. Mikheeva, J. N. Andersen, M. K. J. Johansson, G. Chiaia, T. Rogelet, S. Söderholm, O. Tjernberg, H. Nylén, I. Lindau, R. Nyholm, U. O. Karlsson, S. N. Barilo, and S. V. Shiryaev, Photoemission and x-ray absorption study of superconducting and semiconducting $Ba_{1-x}K_xBiO_3$ single crystals, Phys. Rev. B **54**, 6700 (1996).

[25] N. C. Plumb, D. J. Gawryluk, Y. Wang, Z. Ristić, J. Park, B. Q. Lv, Z. Wang, C. E. Matt, N. Xu, T. Shang, K. Conder, J. Mesot, S. Johnston, M. Shi, and M. Radović, Momentum-resolved electronic structure of the high-T_c superconductor parent compound $BaBiO_3$, Phys. Rev. Lett. **117**, 037002 (2016).

[26] L. F. Mattheiss and D. R. Hamann, Electronic- and crystal-structure effects on superconductivity in the $BaPb_{1-x}Bi_xO_3$ system, Phys. Rev. B **26**, 2686 (1982).

[27] L. F. Mattheiss and D. R. Hamann, Electronic structure of $BaPb_{1-x}Bi_xO_3$, Phys. Rev. B **28**, 4227 (1983).

[28] A. Khazraie, K. Foyevtsova, I. Elfimov, and G. A. Sawatzky, Oxygen holes and hybridization in the bismuthates, Phys. Rev. B **97**, 075103 (2018).

[29] G. M. Dalpian, Q. Liu, J. Varignon, M. Bibes, and A. Zunger, Bond disproportionation, charge self-regulation, and ligand holes in *s-p* and in *d*-electron ABX_3 perovskites by density functional theory, Phys. Rev. B **98**, 075135 (2018).

[30] E. Jurczek and T. M. Rice, A charge-density-wave instability in $BaBi_{1-x}Pb_xO_3$ caused by strong electron-phonon coupling, Europhys. Lett. **1**, 225 (1986).

[31] S. Tajima, S. Uchida, A. Masaki, H. Takagi, K. Kitazawa, S. Tanaka, and A. Katsui, Optical study of the metal-semiconductor transition in $BaPb_{1-x}Bi_xO_3$, Phys. Rev. B **32**, 6302 (1985).

[32] S. Tajima, S. Uchida, A. Masaki, H. Takagi, K. Kitazawa, S. Tanaka, and S. Sugai, Electronic states of $BaPb_{1-x}Bi_xO_3$ in the semiconducting phase investigated by optical measurements, Phys. Rev. B **35**, 696 (1987).

[33] M. Merz, N. Nücker, S. Schuppler, D. Arena, J. Dvorak, Y. U. Idzerda, S. N. Ustinovich, A. G. Soldatov, S. V. Shiryaev, and S. N. Barilo, X-ray absorption of $Ba_{1-x}K_xBiO_3$ and $BaPb_{1-y}Bi_yO_3$: Competition between bipolaronic and charge-density wave states, Europhys. Lett. **72**, 275 (2005).

[34] A. Menushenkov, A. Ignatov, K. Klementev, and D. Kochubey, X-ray absorption spectroscopy of $BaPb_{1-x}Bi_xO_{3-\delta}$ and $Ba_{1-x}K_xBiO_{3-\delta}$ superconducting oxides, Phys. B: Condens. Matter **208-209**, 295 (1995).

[35] A. Ignatov, A. Menushenkov, and V. Chernov, Influence of oxygen deficiency on the electronic and local structure of $BaPb_{1-x}Bi_xO_{3-\delta}$ and $Ba_{0.6}K_{0.4}BiO_{3-\delta}$ superconducting oxides: an X-ray absorption study, Physica C **271**, 32 (1996).

[36] A. Ignatov, Relationship between the electronic and local structure in $BaPb_xBi_{1-x}O_3$ and $Ba_{1-x}K_xO_3$ perovskites, Nucl. Instrum. Methods Phys. Res. Sect. A **448**, 332 (2000).

[37] K. Foyevtsova, A. Khazraie, I. Elfimov, and G. A. Sawatzky, Hybridization effects and bond disproportionation in the bismuth perovskites, Phys. Rev. B **91**, 121114(R) (2015).

[38] M. Bharath, P. Sharma, J. Brar, R. K. Maurya, and R. Bindu, Interplay of lattice distortion and electronic structure in $BaBiO_3$, J. Phys.: Condens. Matter **32**, 055504 (2020).

[39] A. P. Menushenkov and K. V. Klementev, Extended x-ray absorption fine-structure indication of a double-well potential for oxygen vibration in $Ba_{1-x}K_xBiO_3$, J. Phys.: Condens. Matter **12**, 3767 (2000).

[40] A. P. Menushenkov, K. V. Klement'ev, P. V. Konarev, and A. A. Meshkov, Anharmonicity and superconductivity in $Ba_{0.6}K_{0.4}BiO_3$, JETP Lett. **67**, 1034 (1998).

[41] N. Mott, Real space bosons in the bismuth oxide and copper oxide superconductors, Supercond. Sci. Technol. **4**, S59 (1991).

[42] A. Taraphder, H. R. Krishnamurthy, R. Pandit, and T. V. Ramakrishnan, Negative-*U* extended Hubbard model for doped barium bismuthates, Phys. Rev. B **52**, 1368 (1995).

[43] C. M. Varma, Missing valence states, diamagnetic insulators, and superconductors, Phys. Rev. Lett. **61**, 2713 (1988).

[44] A. Taraphder, R. Pandit, H. R. Krishnamurthy, and T. V. Ramakrishnan, The exotic barium bismuthates, Int. J. Mod. Phys. B **10**, 863 (1996).

[45] R. Micnas, J. Ranninger, and S. Robaszkiewicz, Superconductivity in narrow-band systems with local nonretarded attractive interactions, Rev. Mod. Phys. **62**, 113 (1990).

[46] I. B. Bischofs, V. N. Kostur, and P. B. Allen, Polaron and bipolaron defects in a charge density wave: A model for lightly doped $BaBiO_3$, Phys. Rev. B **65**, 115112 (2002).

[47] A. P. Menushenkov, I. A. Troyan, and M. I. Eremets, Resonant Raman scattering in superconducting $Ba_{1-x}K_xBiO_3$, JETP Lett. **77**, 521 (2003).

[48] A. P. Menushenkov, K. V. Klementev, A. V. Kuznetsov, and M. Y. Kagan, Superconductivity in $Ba_{1-x}K_xBiO_3$: Possible scenario of spatially separated Fermi-Bose mixture, J. Exp. Theor. Phys. **93**, 615 (2001).

[49] A. P. Menushenkov, A. V. Kuznetsov, K. V. Klementiev, and M. Y. Kagan, Fermi-bose mixture in $Ba(K)BiO_3$ superconducting oxide, J. Supercond. Novel Magn. **29**, 701 (2016).

[50] R. Mankowsky, M. Fechner, M. Först, A. von Hoegen, J. Porras, T. Loew, G. L. Dakovski, M. Seaberg, S. Möller, G. Coslovich,

B. Keimer, S. S. Dhesi, and A. Cavalleri, Optically induced lattice deformations, electronic structure changes, and enhanced superconductivity in $YBa_2Cu_3O_{6.48}$, Struct. Dyn. **4**, 044007 (2017).

[51] M. Mitrano, S. Lee, A. A. Husain, L. Delacretaz, M. Zhu, G. de la Peña Munoz, S. X.-L. Sun, Y. I. Joe, A. H. Reid, S. F. Wandel, G. Coslovich, W. Schlotter, T. van Driel, J. Schneeloch, G. D. Gu, S. Hartnoll, N. Goldenfeld, and P. Abbamonte, Ultrafast time-resolved x-ray scattering reveals diffusive charge order dynamics in $La_{2-x}Ba_xCuO_4$, Sci. Adv. **5**, eaax3346 (2019).

[52] D. R. Baykusheva, H. Jang, A. A. Husain, S. Lee, S. F. R. TenHuisen, P. Zhou, S. Park, H. Kim, J.-K. Kim, H.-D. Kim, M. Kim, S.-Y. Park, P. Abbamonte, B. J. Kim, G. D. Gu, Y. Wang, and M. Mitrano, Ultrafast renormalization of the on-site coulomb repulsion in a cuprate superconductor, Phys. Rev. X **12**, 011013 (2022).

[53] H. Jang, S. Song, T. Kihara, Y. Liu, S.-J. Lee, S.-Y. Park, M. Kim, H.-D. Kim, G. Coslovich, S. Nakata, Y. Kubota, I. Inoue, K. Tamasaku, M. Yabashi, H. Lee, C. Song, H. Nojiri, B. Keimer, C.-C. Kao, and J.-S. Lee, Characterization of photoinduced normal state through charge density wave in superconducting $YBaCu_3O_{6.67}$, Sci. Adv. **8**, (2022).

[54] L. L. Guyader, A. Eschenlohr, M. Beye, W. Schlotter, F. Döring, C. Carinan, D. Hickin, N. Agarwal, C. Boeglin, U. Bovensiepen, J. Buck, R. Carley, A. Castoldi, A. D'Elia, J.-T. Delitz, W. Ehsan, R. Engel, F. Erdinger, H. Fangohr, P. Fischer *et al.*, Photon-shot-noise-limited transient absorption soft X-ray spectroscopy at the European XFEL, J. Synchrotron Rad. **30**, 284 (2023).

[55] N. Gerasimova, D. L. Civita, L. Samoylova, M. Vannoni, R. Villanueva, D. Hickin, R. Carley, R. Gort, B. E. V. Kuiken, P. Miedema, L. L. Guyarder, L. Mercadier, G. Mercurio, J. Schlappa, M. Teichman, A. Yaroslavtsev, H. Sinn, and A. Scherz, The soft X-ray monochromator at the SASE3 beamline of the European XFEL: From design to operation, J. Synchrotron Rad. **29**, 1299 (2022).

[56] K. Kobayashi, T. Mizokawa, A. Ino, J. Matsuno, A. Fujimori, H. Samata, A. Mishiro, Y. Nagata, and F. M. F. de Groot, Doping dependence of the electronic structure of $Ba_{1-x}K_xBiO_3$ studied by x-ray-absorption spectroscopy, Phys. Rev. B **59**, 15100 (1999).

[57] See Supplemental Material at http://link.aps.org/supplemental/10.1103/PhysRevResearch.6.023307 for details on *ab initio* calculations; three-exponential model; and sample preparation.

[58] A. E. Lukyanov, V. D. Neverov, Y. V. Zhumagulov, A. P. Menushenkov, A. V. Krasavin, and A. Vagov, Laser-induced ultrafast insulator-metal transition in $BaBiO_3$, Phys. Rev. Res. **2**, 043207 (2020).

[59] It should be noted that conventional DFT calculations, being the one-particle approach, do not allow one to adequately describe the intermediate stage of the process of rapid rearrangement of local electronic and crystal structures, shown in Fig. 6. Apparently, this is the main reason for the previously noted discrepancy between the results of DFT and other types of calculations and the results of experiments. In the mentioned Ref. [58], the lattice of octahedrons of different sizes was created manually before running the DFT calculations.

[60] H. Namatame, A. Fujimori, H. Takagi, S. Uchida, F. M. F. de Groot, and J. C. Fuggle, Electronic structure and the metal-semiconductor transition in $BaPb_{1-x}Bi_xO_3$ studied by photoemission and x-ray-absorption spectroscopy, Phys. Rev. B **48**, 16917 (1993).

[61] S. Sugai, Dimerization model for the metal-semiconductor transition in $BaPb_{1-x}Bi_xO_3$, Phys. Rev. B **35**, 3621 (1987).

[62] D. F. Agterberg, J. S. Davis, S. D. Edkins, E. Fradkin, D. J. V. Harlingen, S. A. Kivelson, P. A. Lee, L. Radzihovsky, J. M. Tranquada, and Y. Wang, The physics of pair-density waves: Cuprate superconductors and beyond, Annu. Rev. Condens. Matter Phys. **11**, 231 (2020).

[63] I. Božović and J. Levy, Pre-formed Cooper pairs in copper oxides and $LaAlO_3-SrTiO_3$ heterostructures, Nat. Phys. **16**, 712 (2020).

[64] K. M. Bastiaans, D. Chatzopoulos, J.-F. Ge, D. Cho, W. O. Tromp, J. M. van Ruitenbeek, M. H. Fischer, P. J. de Visser, D. J. Thoen, E. F. C. Driessen, T. M. Klapwijk, and M. P. Allan, Direct evidence for Cooper pairing without a spectral gap in a disordered superconductor above T_c, Science **374**, 608 (2021).

[65] G. Cheng, M. Tomczyk, S. Lu, J. P. Veazey, M. Huang, P. Irvin, S. Ryu, H. Lee, C.-B. Eom, C. S. Hellberg, and J. Levy, Electron pairing without superconductivity, Nature (London) **521**, 196 (2015).

[66] D. M. Eagles, Possible pairing without superconductivity at low carrier concentrations in bulk and thin-film superconducting semiconductors, Phys. Rev. **186**, 456 (1969).

[67] S. Salem-Sugui, E. E. Alp, S. M. Mini, M. Ramanathan, J. C. Campuzano, G. Jennings, M. Faiz, S. Pei, B. Dabrowski, Y. Zheng, D. R. Richards, and D. G. Hinks, Determination of the local structure in $Ba_{1-x}K_xBiO_3$ by x-ray-absorption spectroscopy, Phys. Rev. B **43**, 5511 (1991).

[68] T. J. Wagener, H. M. Meyer, D. M. Hill, Y. Hu, M. B. Jost, J. H. Weaver, D. G. Hinks, B. Dabrowski, and D. R. Richards, Photoemission and inverse-photoemission studies of $Ba_{1-x}K_xBiO_{3-y}$, Phys. Rev. B **40**, 4532 (1989).

[69] W. R. Pudelko, A. Krzton-Maziopa, A. Lynnyk, R. Puzniak, K. Lawniczak-Jablonska, D. J. Gawryluk, D. Moszczynska, and J. Mizera, Bismuth and oxygen valencies and superconducting state properties in $Ba_{1-x}K_xBiO_3$ superconductor, Phys. B: Condens. Matter **591**, 412226 (2020).

[70] C. Yang, Y. Liu, Y. Wang, L. Feng, Q. He, J. Sun, Y. Tang, C. Wu, J. Xiong, W. Zhang, X. Lin, H. Yao, H. Liu, G. Fernandes, J. Xu, J. M. Valles, J. Wang, and Y. Li, Intermediate bosonic metallic state in the superconductor-insulator transition, Science **366**, 1505 (2019).

[71] C. Yang, H. Liu, Y. Liu, J. Wang, D. Qiu, S. Wang, Y. Wang, Q. He, X. Li, P. Li, Y. Tang, J. Wang, X. C. Xie, J. M. Valles, J. Xiong, and Y. Li, Signatures of a strange metal in a bosonic system, Nature (London) **601**, 205 (2022).

[72] A. W. Sleight, Bismuthates: $BaBiO_3$ and related superconducting phases, Physica C **514**, 152 (2015).

[73] A. R. Bishop, D. Mihailovic, and J. Mustre de León, Signatures of mesoscopic Jahn Teller polaron inhomogeneities in high-temperature superconductors, J. Phys.: Condens. Matter **15**, L169 (2003).

[74] A. Menushenkov, A. Kuznetsov, R. Chernikov, A. Ivanov, V. Sidorov, and K. Klementiev, Correlation of the local and the macroscopic properties of high-temperature superconductors, Z. Kristallogr. **225**, 487 (2010).

[75] A. P. Menushenkov, A. V. Kuznetsov, R. V. Chernikov, A. A. Ivanov, V. V. Sidorov, and K. V. Klementiev, Role of the

perovskite-like lattice in the high-temperature superconductor mechanism: EXAFS data analysis, J. Surf. Invest. **7**, 407 (2013).

[76] V. Velasco, M. B. Silva Neto, A. Perali, S. Wimberger, A. R. Bishop, and S. D. Conradson, Kuramoto synchronization of quantum tunneling polarons for describing the dynamic structure in cuprate superconductors, Phys. Rev. B **105**, 174305 (2022).

[77] J.-Y. Oh, D.-S. Yang, and B. Kang, Local instability in $GdBa_2Cu_3O_{7-x}/La_{0.7}Sr_{0.3}MnO_3$ superconducting bilayer: Temperature-dependent EXAFS study, Ceram. Int. **49**, 25767 (2023).

[78] V. Velasco, M. B. S. Neto, A. Perali, S. Wimberger, A. R. Bishop, and S. D. Conradson, Evolution of charge-lattice dynamics across the kuramoto synchronization phase diagram of quantum tunneling polarons in cuprate superconductors, Condens. Matter **6**, 52 (2021).

[79] K. A. Müller, G. Zhao, K. Conder, and H. Keller, The ratio of small polarons to free carriers in derived from susceptibility measurements, J. Phys.: Condens. Matter **10**, L291 (1998).

[80] M. Kim, G. M. McNally, H.-H. Kim, M. Oudah, A. S. Gibbs, P. Manuel, R. J. Green, R. Sutarto, T. Takayama, A. Yaresko, U. Wedig, M. Isobe, R. K. Kremer, D. A. Bonn, B. Keimer, and H. Takagi, Superconductivity in (Ba, K)SbO_3, Nat. Mater. **21**, 627 (2022).

[81] A. Menushenkov, Correlation of the local and the macroscopic properties of high-temperature superconductors: EXAFS data analysis, J. Synchrotron Radiat. **10**, 369 (2003).

[82] M. Porro, L. Andricek, S. Aschauer, A. Castoldi, M. Donato, J. Engelke, F. Erdinger, C. Fiorini, P. Fischer, H. Graafsma, A. Grande, C. Guazzoni, K. Hansen, S. Hauf, P. Kalavakuru, H. Klaer, M. Tangl, A. Kugel, M. Kuster, P. Lechner *et al.*, The MiniSDD-based 1-mpixel camera of the DSSC project for the european XFEL, IEEE Trans. Nucl. Sci. **68**, 1334 (2021).

[83] G. Kim, M. Neumann, M. Kim, M. D. Le, T. D. Kang, and T. W. Noh, Suppression of three-dimensional charge density wave ordering via thickness control, Phys. Rev. Lett. **115**, 226402 (2015).

[84] P. Blaha, K. Schwarz, F. Tran, R. Laskowski, G. K. H. Madsen, and L. D. Marks, WIEN2k: An APW+lo program for calculating the properties of solids, J. Chem. Phys. **152**, 074101 (2020).

[85] B. J. Kennedy, C. J. Howard, K. S. Knight, Z. Zhang, and Q. Zhou, Structures and phase transitions in the ordered double perovskites $Ba_2Bi^{III}Bi^{V}O_6$ and $Ba_2Bi^{III}Sb^{V}O_6$, Acta Crystallogr. B: Struct. Sci. **62**, 537 (2006).